

Spin-Polaron Mediated Superconductivity in Doped Chern Antiferromagnets

Xuepeng Wang,¹ J. F. Mendez-Valderrama,¹ Johannes S. Hofmann,^{2,*} and Debanjan Chowdhury^{1,†}

¹*Department of Physics, Cornell University, Ithaca, New York 14853, USA.*

²*Max-Planck-Institut für Physik Komplexer Systeme,
Nöthnitzer Strasse 38, 01187 Dresden, Germany*

(Dated: August 1, 2025)

The study of interacting topological bands with a tunable bandwidth offers a unique platform to study the interplay of intertwined orders and emergent non-electronic excitations. Here we design a time-reversal symmetric and sign-problem-free electronic model with tunable Chern bands carrying valley-contrasting Chern number, interacting via competing (anti-)ferromagnetic interactions. Using numerically exact quantum Monte-Carlo computations, we analyze the many-body phase-diagram as a function of temperature and band filling fractions over a wide range of electronic bandwidth, interaction anisotropy, and an Ising spin-orbit coupling. At a commensurate filling of the Chern bands, the ground state hosts intra-valley ferromagnetic coherence and inter-valley antiferromagnetism, thus realizing an insulating Chern antiferromagnet (CAF). Upon doping, the ground-state develops superconductivity, but where the low-energy charged quasiparticles are composite objects — electrons dressed by multiple spin-flip excitations. These spin-polaron (or skyrmion) excitations persist in the presence of a weak spin-orbit coupling. In a companion article [1], we address the emergent symmetries and low-energy field-theoretic aspects of the problem and reveal the proximity to a deconfined quantum critical point. We end by providing a general outlook towards building microscopic connections with models of interacting moiré materials, including twisted bilayer graphene, where many of the ingredients considered here are naturally present.

Introduction.— Two remarkable examples of correlated electronic systems that have captivated researchers at the frontiers of condensed matter physics over the past few decades are quantum Hall systems [2] and lightly-doped Mott insulators with emergent local moments [3]. The study of quantum Hall phases in interacting Landau levels has revealed extraordinary topological properties [4], including exotic collective excitations like skyrmions [5] — nontrivial spin textures that carry electron charge. Meanwhile, lightly doped Mott insulators have demonstrated the emergence of high-temperature superconductivity from repulsive interactions, alongside various intertwined quantum orders [6]. The recent discovery of a variety of moiré materials [7, 8], with their tunable Chern bands, offers an exciting new experimental platform that elegantly bridges these two paradigmatic systems [9–11], opening fresh avenues for exploration at their intersection.

Interactions projected onto nearly flat, isolated topological bands can drive a remarkable array of correlated phenomena. A particularly elegant — and perhaps counterintuitive — example is the emergence of superconductivity in isolated flat bands [12], made possible by the complex spatial distribution of Bloch wavefunctions and interaction-driven delocalization of Cooper pairs. This superconducting mechanism operates in an intermediate to strong-coupling regime that fundamentally transcends the conventional Bardeen-Cooper-Schrieffer framework, though a variety of recent non-perturbative theoretical investigations of flat-band superconductivity have found that the Cooper pairs can still originate from underlying electrons [13–17]. On the other hand, previous research has proposed that composite quasiparticles such as

skyrmions (or spin-polarons, corresponding to electrons dressed by spin-flip excitations) may facilitate superconductivity when doped away from various correlated insulators in topological settings [18–20], or near deconfined quantum critical points [21–24]. Nevertheless, our microscopic understanding of how superconductivity emerges at a finite temperature from a parent metallic state beyond solvable Landau-level-like systems remains limited, particularly in contexts where controlled theoretical approaches are unavailable.

In this letter, we critically examine how topology enables spin-polarons or skyrmions (terms we use interchangeably and characterize precisely below) to emerge as the lowest energy excitations in microscopic systems distinctly removed from Landau-level-like regimes. Furthermore, we will also investigate how the superconducting transition temperature is affected due to the underlying competing ordering tendencies when doped away from Mott insulating states at commensurate band fillings. Our analysis centers on a time-reversal symmetric model of Chern bands incorporating both spin and “valley” degrees of freedom, governed by repulsive interactions and characterized by the following microscopic symmetries: $U(1)_{\text{charge}} \times U(1)_{\text{valley}} \times SU(2)_{\text{spin}}$. Our investigation begins with a lattice model of interacting Chern bands featuring tunable bandwidth, which we analyze for a range of band-fillings and temperature. Instead of incorporating the full Coulomb interactions, we focus on a specialized limit examining the interplay between an intra-valley ferromagnetic interaction, J_H , arising from an underlying Hund’s-type coupling and inter-valley antiferromagnetic interactions, J_A , generated through inter-valley superexchange. This carefully con-

structured model circumvents the notorious fermion sign-problem, enabling numerically exact solutions via determinant quantum Monte Carlo (DQMC) [25–27] across an extensive parameter space, that includes the band-filling, the bandwidth and the ratio $|J_H|/J_A$.

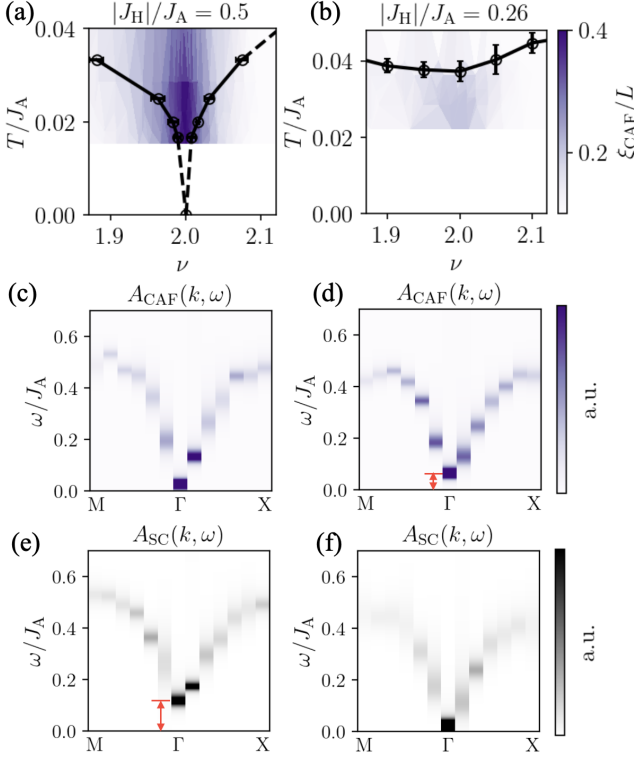


FIG. 1. Many-body phase diagram for $\mathcal{F} = 0.01$ at $\nu = 2$ with: (a) $|J_H|/J_A = 0.5$, and (b) $|J_H|/J_A = 0.26$. Black data points represent T_c^{SC} obtained using the BKT criterion [28] and scaling analysis [29]; solid lines serve as a guide to the eye. The purple shading represents the normalized CAF correlation length, ξ_{CAF}/L . Two-particle spectral function, $A_\lambda(\mathbf{k}, \omega)$, at $\nu = 2$ and $T = 0$ obtained from stochastic analytical continuation for $\lambda \equiv \text{CAF}$ (Eq. (3b)) for (c) $|J_H|/J_A = 0.5$ shows Goldstone mode(s), and (d) for $|J_H|/J_A = 0.26$ shows gapped excitation. Similarly, for $\lambda \equiv \text{SC}$, the spectral function shows (e) a gapped spectrum for $|J_H|/J_A = 0.5$, and (f) a Goldstone mode for $|J_H|/J_A = 0.26$. Red arrows in (d) and (e) denote the gap in the two-particle spectra.

We have observed that the system exhibits a strong tendency to spontaneously break the $SU(2)_{\text{spin}}$ symmetry at half-filling of the isolated electronic bands, reminiscent of quantum Hall ferromagnetism. Notably, this occurs despite fundamental differences from the spinful Landau-level problem — our bands are not flat, the berry curvature distribution in momentum-space is non-uniform, the quantum geometry deviates from the ideal trace condition, and the interaction strength is comparable in magnitude to the gap to remote bands. The resulting ground state manifests as an insulating intra-valley Chern ferromagnet, with time-reversed valleys ordered

in a relative antiferromagnetic configuration. Upon doping, electronic charge enters each valley as spin-polarons, while intervalley antiferromagnetic exchange binds these charge e spin-polarons into Cooper pairs, yielding superconductivity [18]. Our investigation reveals the effect of varying electronic bandwidth and the relative ratio $|J_H|/J_A$ on the stability of the insulating Chern antiferromagnet, the energetics of charged excitations, and superconductivity. We also present results obtained using DQMC on the collective mode spectra and the impact of spin-orbit coupling on the spin-polaron phenomenology and superconductivity. In a companion article [1] we address the low-energy field theoretic structure — including an emergent $SO(5)$ symmetry and a proximity to deconfined quantum criticality — alongside Hartree-Fock treatment for the same microscopic model, revealing complementary insights on many of the fundamental questions raised here.

Model.— We work with a time-reversal symmetric model of interacting topological bands with Chern number, $C = \pm 1$ in two-dimensions. Microscopically, the degrees of freedom consist of spin ($\sigma = \uparrow, \downarrow$), a fictitious “valley” ($\tau = \pm$) and sublattice ($\eta = A, B$), such that the non-interacting part of the Hamiltonian per valley, $H_{\text{kin}}^{(\tau)}$, in momentum space is of the form [13, 30, 31],

$$H_{\text{kin}}^{(\tau)} = \sum_{\mathbf{k}} \psi_{\mathbf{k},\tau}^\dagger \left[B_{\mathbf{k},\tau}^0 \eta_0 + \mathbf{B}_{\mathbf{k},\tau} \cdot \boldsymbol{\eta} \right] \sigma_0 \psi_{\mathbf{k},\tau}, \quad (1)$$

where $\psi_{\mathbf{k},\tau}^\dagger = (c_{\mathbf{k},A,\tau,\uparrow}^\dagger, c_{\mathbf{k},B,\tau,\uparrow}^\dagger, c_{\mathbf{k},A,\tau,\downarrow}^\dagger, c_{\mathbf{k},B,\tau,\downarrow}^\dagger)$ and $c_{\mathbf{k},\eta,\tau,\sigma}^\dagger$ denotes the electron creation operator on sublattice η with spin σ and valley τ . The matrices $B_{\mathbf{k},\tau}^0$ and $\mathbf{B}_{\mathbf{k},\tau}$ are fixed by the tight-binding parameters on an underlying lattice. For simplicity, we assume a square lattice model with a first (t) and staggered second neighbor hopping ($t_2 = t/\sqrt{2}$) with a π -flux per square plaquette [29]. In order to tune the electronic bandwidth, we can include further (e.g. a fifth, t_5) neighbor hopping, which helps tune the flatness ratio $\mathcal{F} = W/E_{\text{gap}}$ ($W \equiv$ bandwidth, $E_{\text{gap}} \equiv$ remote bandgap) to be small. We construct two copies of $H_{\text{kin}}^{(\tau)}$ in a time-reversal-invariant fashion [29], under the operation $\mathcal{T} = i\tau_y \mathcal{K}$ where \mathcal{K} denotes complex conjugation. This yields a model with a set of degenerate topological bands carrying spin and valley with $C = \tau$.

In our previous discussion, we presented two competing local magnetic interactions: a ferromagnetic intra-valley Hund’s interaction with $J_H < 0$ and an antiferromagnetic inter-valley exchange with $J_A > 0$. We will examine how these interactions once effectively projected to the low-energy Chern bands influence the competition between spontaneously symmetry-broken phases at commensurate fillings and superconductivity in our proposed model. While these interaction forms draw partial inspiration from quantum Hall ferromagnetism

in spinful Landau levels [32–35], our framework operates well beyond any readily “solvable” quantum Hall regime. The interactions take the form, $H_{\text{interaction}} = H_{\text{intra-valley}} + H_{\text{inter-valley}}$, where

$$H_{\text{intra-valley}} = -|J_H| \sum_{\mathbf{r}, \tau=\pm} \mathbf{S}_{\mathbf{r}}^{\tau} \cdot \mathbf{S}_{\mathbf{r}}^{\tau}, \quad (2a)$$

$$H_{\text{inter-valley}} = J_A \sum_{\mathbf{r}} \mathbf{S}_{\mathbf{r}}^{+} \cdot \mathbf{S}_{\mathbf{r}}^{-}, \quad \text{where} \quad (2b)$$

$$\mathbf{S}_{\mathbf{r}}^{\tau} = \sum_{\alpha, \beta=\uparrow, \downarrow} c_{\mathbf{r}, \tau, \alpha}^{\dagger} \boldsymbol{\sigma}_{\alpha\beta} c_{\mathbf{r}, \tau, \beta}. \quad (2c)$$

Note that we combine the sublattice index (η) into the two-dimensional spatial coordinate \mathbf{r} .

Quantum Monte Carlo Simulations.- Our proposed model features an anti-unitary time-reversal symmetry, $\mathcal{T}' = i\tau_x \sigma_y \mathcal{K}$, which allows for sign-problem-free DQMC at *any* filling fraction ν , provided that $J_A \geq 2|J_H|$. We evaluate the partition function for the model defined by $H = (\sum_{\tau} H_{\text{kin}}^{(\tau)} + H_{\text{interaction}})$ using a Trotter decomposition with $\Delta\tau = \beta/N_{\text{Trotter}}$; the interaction terms are factorized through a discrete Hubbard-Stratonovich transformation, with auxiliary fields sampled stochastically via single spin-flip updates. We will analyze the low temperature phase diagram and the low-energy excitation spectrum for a range of bare band dispersion, $\mathcal{F} = 0.01 - 0.2$, and for interaction strengths $J_A/E_{\text{gap}} = 0.625$, where $E_{\text{gap}} = 4t$. We determine the band-filling by adjusting the chemical potential $\mu(T)$ to satisfy $\sum_{\mathbf{r}} \langle n_{\mathbf{r}} \rangle / L^2 = \nu$, where ν represents the total filling and $n_{\mathbf{r}} = \sum_{\tau, \sigma} c_{\mathbf{r}, \tau, \sigma}^{\dagger} c_{\mathbf{r}, \tau, \sigma}$ represents the local electron density ($L^2 \equiv$ system size). In the parameter regime where the model is sign-problem free, the inter-valley antiferromagnetic exchange is large relative to the intra-valley ferromagnetic exchange; we focus primarily on the limit $J_A = 2|J_H|$ in the remainder of this study where the Hunds’ interaction relative to the antiferromagnetic exchange is maximized. However, we have also observed interesting quantum phase transitions as a function of decreasing $|J_H|/J_A$ at a fixed $\nu = 2$, reminiscent of deconfined quantum criticality with emergent $SO(5)$ symmetry [1].

Phase-diagram.- Let us start by discussing the many-body phase diagram for $\mathcal{F} = 0.01$. The candidate order-parameters of interest are a spin-singlet valley-triplet ($\tau_z = 0$) superconductivity and a Chern-antiferromagnet (CAF) defined as,

$$O_{\text{SC}} \equiv c_{\mathbf{r}+\uparrow}^{\dagger} c_{\mathbf{r}-\downarrow}^{\dagger} - c_{\mathbf{r}+\downarrow}^{\dagger} c_{\mathbf{r}-\uparrow}^{\dagger}, \quad (3a)$$

$$O_{\text{CAF}}^{\alpha} \equiv \psi_{\mathbf{r}}^{\dagger} \sigma^{\alpha} \tau^z \psi_{\mathbf{r}}, \quad (\alpha = 1, 2, 3). \quad (3b)$$

We use the Berezinskii–Kosterlitz–Thouless (BKT) criterion [36, 37] and scaling analysis to determine the superconducting transition temperature T_c^{SC} [29]. The data for T_c^{SC} is shown in Fig. 1(a)-(b) for two different values

of $|J_H|/J_A$ in the vicinity of $\nu = 2$; the superconducting pairing symmetry is given by Eq. 3a.

We find that for $|J_H|/J_A = 0.5$, which lies at the boundary of parameter-space where the sign-problem is absent, the superconducting $T_c^{\text{SC}} \rightarrow 0$ as $\nu \rightarrow 2$; see Fig. 1(a). The ground state at $\nu = 2$ is an insulating CAF [1] with an order-parameter described by Eq. 3b. At a finite temperature and for $|J_H|/J_A = 0.5$, the CAF correlation length, ξ_{CAF} , shows a strong enhancement upon approaching $\nu = 2$ as a function of decreasing temperature, as shown in Fig. 1(a). However, the CAF at $\nu = 2$ is restricted to only a certain range of accessible $|J_H|/J_A$. For instance, when $|J_H|/J_A = 0.26$, the superconducting T_c^{SC} is finite in the entire neighborhood of $\nu = 2$; see Fig. 1(b). Interestingly, there is still a small enhancement in ξ_{CAF} near $\nu = 2$ for $|J_H|/J_A = 0.26$, which has a rather weak effect on T_c^{SC} , as seen in Fig. 1(b).

By performing a $T = 0$ projective quantum Monte-Carlo computation, we have established that the $\nu = 2$ ground state for $|J_H|/J_A = 0.5$ is a CAF [1]. This is corroborated by analyzing the spectral properties (after analytic continuation to real frequencies) of two-point correlation functions involving the order-parameters introduced above. Specifically, by analyzing the frequency and momentum-resolved spectral function, $A_{\lambda}(\mathbf{k}, \omega) = \text{Im} \langle O_{\lambda}^{\dagger}(\mathbf{k}, \omega) O_{\lambda}(\mathbf{k}, \omega) \rangle |_{\omega \rightarrow \omega + i0^{+}}$ ($\lambda \equiv \text{SC, CAF}$), in the limit of $\mathbf{k} \rightarrow 0$, we can identify the gapless Goldstone modes due to the associated spontaneously broken continuous symmetries. For $|J_H|/J_A = 0.5$ and at $\nu = 2$, we observe gapless mode(s) near the Γ -point in the CAF spectral function (Fig. 1c), while for $|J_H|/J_A = 0.26$ the same mode(s) are gapped (Fig. 1d). Relatedly, for $|J_H|/J_A = 0.5$ at $\nu = 2$, the SC spectral function (Fig. 1e) is gapped near the Γ -point, while for $|J_H|/J_A = 0.26$ the same mode is gapless (Fig. 1f). Thus, we have demonstrated that at $\nu = 2$, by simply tuning the ratio $|J_H|/J_A$, we can transit from an insulating Chern antiferromagnet to a superconductor [1].

Charged excitations.- We now examine the evolution of the ground-state when charges are introduced to the incompressible CAF at $\nu = 2$. The observable of interest will be the variation in total spin quantum number, ΔS , as a function of the excess electrons *per valley*. This is reminiscent of the Knight-shift measurements performed in the original quantum Hall setting to reveal the existence of skyrmions [38]. Clearly, if the doped charges enter each valley as a renormalized electronic quasiparticle, the slope should reflect the fundamental $S = 1/2$ quantum number. Conversely, if the lowest energy excitations per valley consist of composite entities involving spin-flips, this will manifest in the slope with $S > 1/2$. Recall that the static spin structure factor *per valley* (τ), $\chi^{\tau}(\mathbf{q})$, can be related to the total (i.e. macroscopic) spin

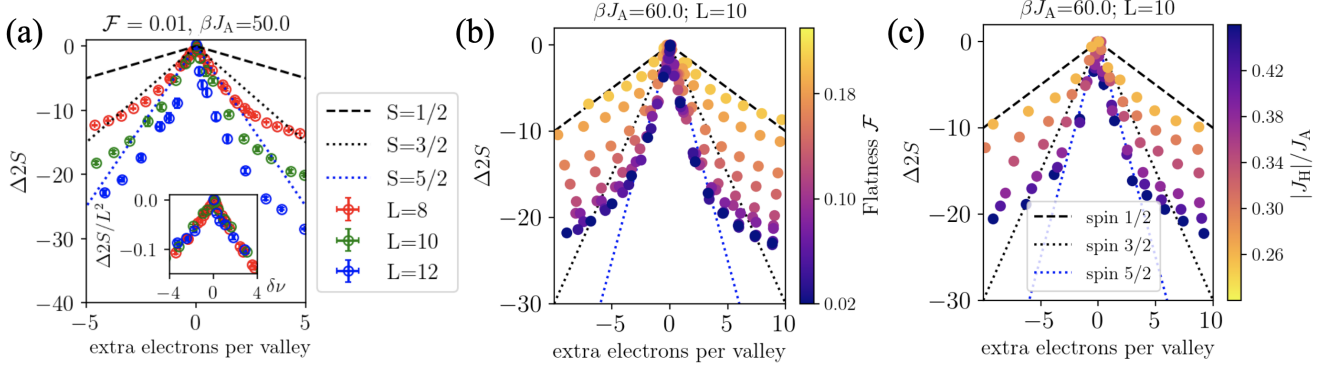


FIG. 2. Evolution of spin quantum number, $\Delta S \equiv S_{\text{tot}}^\tau(\nu) - S_{\text{tot}}^\tau(\nu = 2)$, within a single valley at a fixed: (a) $|J_H|/J_A = 0.5$, $\mathcal{F} = 0.01$ and $\beta J_A = 50$ as a function of increasing linear system size, L , (b) $|J_H|/J_A = 0.5$ and $\beta J_A = 60$ with increasing \mathcal{F} , (c) $\mathcal{F} = 0.01$ and $\beta J_A = 60$ with decreasing $|J_H|/J_A$. Inset of panel (a) shows $(\Delta S/L^2)$, indicating the macroscopic nature of the charged skyrmion excitation.

quantum number S_{tot}^τ per valley via

$$\chi^\tau(\mathbf{q}) = \frac{1}{L^2} \sum_{\mathbf{r}, \mathbf{r}'} e^{-i(\mathbf{r}-\mathbf{r}') \cdot \mathbf{q}} \langle \mathbf{S}^\tau(\mathbf{r}') \cdot \mathbf{S}^\tau(\mathbf{r}) \rangle, \quad (4a)$$

$$\chi^\tau(\mathbf{q} = 0) = S_{\text{tot}}^\tau(S_{\text{tot}}^\tau + 1)/L^2, \quad (4b)$$

where we have dropped some unimportant constant terms. We then compute, $\Delta S \equiv S_{\text{tot}}^\tau(\nu) - S_{\text{tot}}^\tau(\nu = 2)$, defined as the change in the spin quantum number per valley with doping relative to the maximally polarized CAF state at $\nu = 2$ from $\chi^\tau(\mathbf{q} = 0)$.

In Fig. 2, we analyze ΔS as a function of increasing system-size, flatness ratio, \mathcal{F} , and $|J_H|/J_A$. At a fixed $\mathcal{F} = 0.01$, $|J_H|/J_A = 0.5$ and a low temperature $\beta J_A = 50$, we find clear evidence based on ΔS that the doped charge does *not* enter as a $S = 1/2$ electron; see e.g. the strong deviation away from the line with slope $S = 1/2$ in Fig. 2(a). Instead, ΔS appears to involve combinations of $S = 3/2, 5/2, \dots$ excitations, which in turn depend on the system size, $L \times L$. These $S > 1/2$ objects are associated with the electron dressed by multiple spin-flip excitations derived from the intra-valley Chern ferromagnet. If the resulting composite excitation is tightly bound, it is appropriate to describe it as a spin-polaron. However, by studying $(\Delta S/L^2)$ as a function of the total doping summed over *both* valleys, $\delta\nu$, we observe that the charge enters the system as an extended macroscopic object (Inset-Fig. 2a), reminiscent of a skyrmion [5]. We turn next to one of the technical advantages of our setup, which allows us to examine the stability of the insulating phase at $\nu = 2$, and the energetics associated with the doped charges as a function of \mathcal{F} and $|J_H|/J_A$.

With increasing \mathcal{F} at a fixed $|J_H|/J_A$ (Fig. 2b), or decreasing $|J_H|/J_A$ at a fixed \mathcal{F} (Fig. 2c), we continue to observe a substantial parameter space where the $S > 1/2$ skyrmion excitations remain the lowest energy charged excitations, highlighting their stability. The system exhibits a gradual crossover to a regime — when the band-

width is relatively large or the intervalley antiferromagnetic exchange dominates significantly over the intravalley ferromagnetic exchange — where electrons once again become the lowest-energy charged excitations. Our results in Fig. 2(c) also show that with decreasing $|J_H|/J_A$, the tendency towards melting the chern antiferromagnet at $\nu = 2$ decreases the skyrmion size. Remarkably, at $|J_H|/J_A = 0.26$ when the ground state at $\nu = 2$ is a superconductor ($T_c^{\text{SC}}/J_A = 0.037(3)$), the doped charge still enters the system as a skyrmion thereby demonstrating that the mechanism for superconductivity is driven by pairing of a charge- e skyrmion and antiskyrmion, which is also suggestive of an underlying $(|J_H|/J_A)$ -tuned deconfined quantum phase transition [1]. Interestingly, we have seen preliminary tendency towards a non-exponential saturation of the temperature dependence of $\rho_s(T)$ in the lightly doped skyrmion-mediated superconductor, likely due to the presence of the gapless excitations in the proximate CAF phase [29].

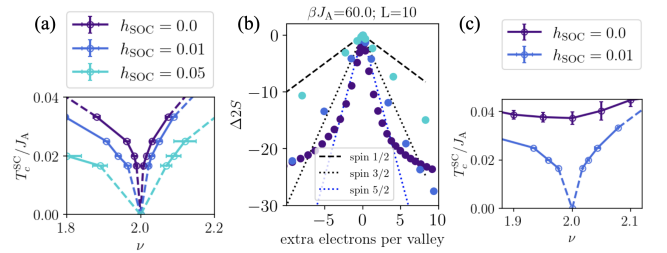


FIG. 3. (a) Many-body phase diagram for $\mathcal{F} = 0.01$ and $|J_H|/J_A = 0.5$ with increasing h_{SOC} . (b) ΔS within a single valley measured relative to $\nu = 2$ with increasing h_{SOC} at $\beta J_A = 60.0$. (c) Evolution of T_c^{SC} with ν for $\mathcal{F} = 0.01$ and $|J_H|/J_A = 0.26$ for $h_{\text{SOC}} \neq 0$.

Effect of spin-orbit coupling.— Our discussion has so far focused on a model with explicit $SU(2)_{\text{spin}}$ symmetry that is broken spontaneously in the CAF phase at $\nu = 2$,

leading to the emergence of skyrmion excitations at $\nu = 2 + \delta\nu$. This naturally raises the question of whether the skyrmions survive if the microscopic $SU(2)_{\text{spin}}$ symmetry is explicitly broken, and how it affects T_c^{SC} . One way to address this question is to include a spin-orbit coupling term at the single-particle level in the Hamiltonian, $H \rightarrow H + H_{\text{SOC}}$,

$$H_{\text{SOC}} = h_{\text{SOC}} \sum_{\mathbf{r}\tau;\alpha,\beta=\uparrow,\downarrow} \tau c_{\mathbf{r},\tau,\alpha}^\dagger \sigma_{\alpha\beta}^z c_{\mathbf{r},\tau,\beta}, \quad (5)$$

without affecting the sign-problem-free property of the full model.

We start by investigating the effect of increasing h_{SOC} on the many-body phase-diagram in the vicinity of $\nu = 2$ for $|J_H|/J_A = 0.5$ and $\mathcal{F} = 0.01$. We find that the insulating phase at $\nu = 2$ survives, and the magnitude of T_c^{SC} obtained by doping away from $\nu = 2$ is suppressed with increasing h_{SOC} ; see Fig. 3(a). The h_{SOC} term breaks the degeneracy between the two contributions to O_{SC} in Eq. 3a and mixes the spin-singlet and spin-triplet superconducting orders. The evolution of ΔS as a function of the doped charge per valley near $\nu = 2$ is shown in Fig. 3(b) as a function of increasing h_{SOC} . Remarkably, the $S > 1/2$ charged excitations still survive at $T \sim h_{\text{SOC}}$, where thermal fluctuations effectively restore the weakly broken $SU(2)_{\text{spin}}$ (due to h_{SOC}). In other words, at these temperatures, the thermally excited skyrmions are the cheapest charged excitations. With increasing h_{SOC} , the skyrmion size decreases culminating in an eventual crossover to ordinary electronic quasiparticles. Finally, in Fig. 3(c), we present the many-body phase-diagram for $|J_H|/J_A = 0.26$ and $\mathcal{F} = 0.01$, where in the absence of h_{SOC} there is no CAF phase. However, with a finite h_{SOC} , the $SU(2)_{\text{spin}}$ degeneracy in the CAF state at $\nu = 2$ is lifted by the spin-orbit coupling, leading to a spin-valley Hall band-insulator. Upon doping, the system develops superconductivity with T_c^{SC} suppressed compared to the $h_{\text{SOC}} = 0$ case. Developing an analytical understanding of why T_c^{SC} is systematically suppressed with increasing h_{SOC} , including when the correlated CAF phase survives at $\nu = 2$, remains an interesting future direction.

Outlook. - Starting from an exactly solvable model with interacting topological bands with a tunable bandwidth, we have demonstrated unambiguous evidence for the presence of composite charged excitations with $S > 1/2$ when doped away from an interaction-induced Chern antiferromagnet at partial commensurate filling. Moreover, the same interactions that generate the insulator also drive pairing of these composite charge excitations to yield a superconductor. We have also demonstrated that the excitations survive in the presence of a weak spin-orbit coupling at a finite temperature. Our findings show a concrete and highly tunable setting at a finite temperature where charged skyrmions-mediated superconductivity has been proposed as a potential mecha-

nism for moiré materials [18, 20, 39–41]. However, we note that our study is in a regime that is far removed from any ideal Landau-level like effective description, due to the finite electronic dispersion, non-concentrated and non-ideal band geometry, and a small interaction-induced mixing with the remote bands. In a companion article [1], we analyze the quantum phase transitions that arise when tuning the bandwidth and interaction anisotropies, and also comment on how the non-ideal band geometry affects the local charged spin-textures.

Our study is inspired by the phenomenology of moiré graphene and some of our findings share a broad conceptual similarity with their microscopic models [42–45], although we do not capture their microscopic bandstructures or the full Coulomb repulsion. It is presently unclear if there are clear experimental signatures of skyrmion-mediated superconductivity in these materials. Interestingly, as a matter of principle, we have demonstrated that a proximity-induced inversion symmetry breaking from a nearby WSe₂ gate [46, 47] does not necessarily suppress the skyrmion excitations altogether. Developing a detailed theory of electrical transport above T_c in the doped metallic state and of the superfluid stiffness far below T_c in the superconducting state remain interesting future research directions. Finding sharp experimental signatures of these skyrmion-like excitations also remains a promising direction.

Acknowledgments. - We thank E. Khalaf and A. Vishwanath for insightful discussions. X.W. thanks J. Dong, P. J. Ledwith and R. Sahay for useful discussions. D.C. is supported in part by a NSF CAREER grant (DMR-2237522), and a Sloan Research Fellowship. D.C. also acknowledges the hospitality of MPI-PKS, Dresden, during the final stages of preparation of this manuscript. This work used Expanse at the San Diego Supercomputer Center through allocation TG-PHY240209 from the Advanced Cyberinfrastructure Coordination Ecosystem: Services & Support (ACCESS) program [48], which is supported by National Science Foundation grants #2138259, #2138286, #2138307, #2137603, and #2138296. The auxiliary field QMC simulations were carried out using the ALF package [27]. This work was supported in part by the Deutsche Forschungsgemeinschaft DFG through the Würzburg-Dresden Cluster of Excellence on Complexity and Topology in Quantum Matter ‘ct.qmat’ (EXC2147, project ID 390858490).

* jhofmann@pks.mpg.de

† debanjanchowdhury@cornell.edu

- [1] X. Wang, J. S. Hofmann, and D. Chowdhury, “Intertwined orders, quantum criticality and skyrmions in tunable topological bands,” (2025).
- [2] S. D. Sarma and A. Pinczuk, *Perspectives in quantum hall effects: Novel quantum liquids in low-dimensional*

- semiconductor structures* (John Wiley & Sons, 2008).
- [3] P. A. Lee, N. Nagaosa, and X.-G. Wen, “Doping a mott insulator: Physics of high-temperature superconductivity,” *Rev. Mod. Phys.* **78**, 17 (2006).
 - [4] B. I. Halperin and J. K. Jain, *Fractional quantum hall effects: new developments* (World Scientific, 2020).
 - [5] S. M. Girvin, “Spin and isospin: Exotic order in quantum hall ferromagnets,” *Physics Today* **53**, 39 (2000).
 - [6] E. Fradkin, S. A. Kivelson, and J. M. Tranquada, “Colloquium: Theory of intertwined orders in high temperature superconductors,” *Rev. Mod. Phys.* **87**, 457 (2015).
 - [7] E. Y. Andrei, D. K. Efetov, P. Jarillo-Herrero, A. H. MacDonald, K. F. Mak, T. Senthil, E. Tutuc, A. Yazdani, and A. F. Young, “The marvels of moiré materials,” *Nature Reviews Materials* **6**, 201 (2021).
 - [8] K. F. Mak and J. Shan, “Semiconductor moiré materials,” *Nature Nanotechnology* **17**, 686 (2022).
 - [9] Y.-H. Zhang and T. Senthil, “Bridging hubbard model physics and quantum hall physics in trilayer graphene/h – BN moiré superlattice,” *Phys. Rev. B* **99**, 205150 (2019).
 - [10] Z.-D. Song and B. A. Bernevig, “Magic-angle twisted bilayer graphene as a topological heavy fermion problem,” *Phys. Rev. Lett.* **129**, 047601 (2022).
 - [11] P. J. Ledwith, J. Dong, A. Vishwanath, and E. Khalaf, “Nonlocal moments and mott semimetal in the chern bands of twisted bilayer graphene,” *Phys. Rev. X* **15**, 021087 (2025).
 - [12] P. Törmä, S. Peotta, and B. A. Bernevig, “Superconductivity, superfluidity and quantum geometry in twisted multilayer systems,” *Nature Reviews Physics* **4**, 528 (2022).
 - [13] J. S. Hofmann, E. Berg, and D. Chowdhury, “Superconductivity, pseudogap, and phase separation in topological flat bands,” *Phys. Rev. B* **102**, 201112 (2020).
 - [14] V. Peri, Z.-D. Song, B. A. Bernevig, and S. D. Huber, “Fragile topology and flat-band superconductivity in the strong-coupling regime,” *Phys. Rev. Lett.* **126**, 027002 (2021).
 - [15] X. Zhang, K. Sun, H. Li, G. Pan, and Z. Y. Meng, “Superconductivity and bosonic fluid emerging from moiré flat bands,” *Phys. Rev. B* **106**, 184517 (2022).
 - [16] J. S. Hofmann, E. Berg, and D. Chowdhury, “Superconductivity, charge density wave, and supersolidity in flat bands with a tunable quantum metric,” *Phys. Rev. Lett.* **130**, 226001 (2023).
 - [17] J. Herzog-Arbeitman, V. Peri, F. Schindler, S. D. Huber, and B. A. Bernevig, “Superfluid Weight Bounds from Symmetry and Quantum Geometry in Flat Bands,” *Physical Review Letters* **128**, 087002 (2022).
 - [18] E. Khalaf, S. Chatterjee, N. Bultinck, M. P. Zaletel, and A. Vishwanath, “Charged skyrmions and topological origin of superconductivity in magic-angle graphene,” *Science Advances* **7**, eabf5299 (2021).
 - [19] M. Christos, S. Sachdev, and M. S. Scheurer, “Superconductivity, correlated insulators, and wess–zumino–witten terms in twisted bilayer graphene,” *Proceedings of the National Academy of Sciences* **117**, 29543 (2020).
 - [20] S. Chatterjee, M. Ippoliti, and M. P. Zaletel, “Skyrmion superconductivity: Dmrg evidence for a topological route to superconductivity,” *Phys. Rev. B* **106**, 035421 (2022).
 - [21] T. Grover and T. Senthil, “Topological spin hall states, charged skyrmions, and superconductivity in two dimensions,” *Phys. Rev. Lett.* **100**, 156804 (2008).
 - [22] Y. Liu, Z. Wang, T. Sato, M. Hohenadler, C. Wang, W. Guo, and F. F. Assaad, “Superconductivity from the condensation of topological defects in a quantum spin-hall insulator,” *Nature Communications* **10**, 2658 (2019).
 - [23] Z. Wang, Y. Liu, T. Sato, M. Hohenadler, C. Wang, W. Guo, and F. F. Assaad, “Doping-induced quantum spin hall insulator to superconductor transition,” *Phys. Rev. Lett.* **126**, 205701 (2021).
 - [24] D. Hou, Y. Liu, T. Sato, W. Guo, F. F. Assaad, and Z. Wang, “Bandwidth-controlled quantum phase transition between an easy-plane quantum spin hall state and an *s*-wave superconductor,” *Phys. Rev. B* **107**, 155107 (2023).
 - [25] F. Becca and S. Sorella, *Quantum Monte Carlo approaches for correlated systems* (Cambridge University Press, 2017).
 - [26] R. Blankenbecler, D. J. Scalapino, and R. L. Sugar, “Monte carlo calculations of coupled boson-fermion systems,” *Phys. Rev. D* **24**, 2278 (1981).
 - [27] F. F. Assaad, M. Bercx, F. Goth, A. Götz, J. S. Hofmann, E. Huffman, Z. Liu, F. P. Toldin, J. S. E. Portela, and J. Schwab, “The ALF (Algorithms for Lattice Fermions) project release 2.0. Documentation for the auxiliary-field quantum Monte Carlo code,” *SciPost Phys. Codebases* , 1 (2022).
 - [28] D. R. Nelson and J. M. Kosterlitz, “Universal jump in the superfluid density of two-dimensional superfluids,” *Phys. Rev. Lett.* **39**, 1201 (1977).
 - [29] “See supplementary material for additional details on the numerical procedures and data.”
 - [30] T. Neupert, L. Santos, C. Chamon, and C. Mudry, “Fractional quantum hall states at zero magnetic field,” *Phys. Rev. Lett.* **106**, 236804 (2011).
 - [31] X. Wang, J. F. Mendez-Valderrama, J. S. Hofmann, and D. Chowdhury, “Intertwined magnetism and superconductivity in isolated correlated flat bands,” *Phys. Rev. B* **110**, L041105 (2024).
 - [32] S. M. Girvin, A. H. MacDonald, and P. M. Platzman, “Magneto-roton theory of collective excitations in the fractional quantum hall effect,” *Phys. Rev. B* **33**, 2481 (1986).
 - [33] S. L. Sondhi, A. Karlhede, S. A. Kivelson, and E. H. Rezayi, “Skyrmions and the crossover from the integer to fractional quantum hall effect at small zeeman energies,” *Phys. Rev. B* **47**, 16419 (1993).
 - [34] K. Moon, H. Mori, K. Yang, S. M. Girvin, A. H. MacDonald, L. Zheng, D. Yoshioka, and S.-C. Zhang, “Spontaneous interlayer coherence in double-layer quantum hall systems: Charged vortices and kosterlitz-thouless phase transitions,” *Phys. Rev. B* **51**, 5138 (1995).
 - [35] S. M. Girvin, “The quantum hall effect: Novel excitations and broken symmetries,” (1999), [arXiv:cond-mat/9907002](https://arxiv.org/abs/cond-mat/9907002) [cond-mat.mes-hall].
 - [36] V. L. Berezinskiĭ, “Destruction of Long-range Order in One-dimensional and Two-dimensional Systems having a Continuous Symmetry Group I. Classical Systems,” *Soviet Journal of Experimental and Theoretical Physics* **32**, 493 (1971).
 - [37] J. M. Kosterlitz and D. J. Thouless, “Ordering, metastability and phase transitions in two-dimensional systems,” *Journal of Physics C: Solid State Physics* **6**, 1181 (1973).
 - [38] S. E. Barrett, G. Dabbagh, L. N. Pfeiffer, K. W. West, and R. Tycko, “Optically pumped nmr evidence for finite-size skyrmions in gaas quantum wells near landau level

- filling $\nu = 1$,” *Phys. Rev. Lett.* **74**, 5112 (1995).
- [39] E. Khalaf and A. Vishwanath, “Baby skyrmions in chern ferromagnets and topological mechanism for spin-polaron formation in twisted bilayer graphene,” *Nature Communications* **13**, 6245 (2022).
 - [40] F. Schindler, O. Vafeck, and B. A. Bernevig, “Trions in twisted bilayer graphene,” *Phys. Rev. B* **105**, 155135 (2022).
 - [41] Y. H. Kwan, G. Wagner, N. Bultinck, S. H. Simon, and S. A. Parameswaran, “Skyrmions in twisted bilayer graphene: Stability, pairing, and crystallization,” *Phys. Rev. X* **12**, 031020 (2022).
 - [42] G. Tarnopolsky, A. J. Kruchkov, and A. Vishwanath, “Origin of Magic Angles in Twisted Bilayer Graphene,” *Phys. Rev. Lett.* **122**, 106405 (2019), publisher: American Physical Society.
 - [43] N. Bultinck, E. Khalaf, S. Liu, S. Chatterjee, A. Vishwanath, and M. P. Zaletel, “Ground State and Hidden Symmetry of Magic-Angle Graphene at Even Integer Filling,” *Phys. Rev. X* **10**, 031034 (2020), publisher: American Physical Society.
 - [44] B. Lian, Z.-D. Song, N. Regnault, D. K. Efetov, A. Yazdani, and B. A. Bernevig, “Twisted bilayer graphene. iv. exact insulator ground states and phase diagram,” *Phys. Rev. B* **103**, 205414 (2021).
 - [45] J. Kang and O. Vafeck, “Strong coupling phases of partially filled twisted bilayer graphene narrow bands,” *Phys. Rev. Lett.* **122**, 246401 (2019).
 - [46] J. Yu, B. A. Foutty, Y. H. Kwan, M. E. Barber, K. Watanabe, T. Taniguchi, Z.-X. Shen, S. A. Parameswaran, and B. E. Feldman, “Spin skyrmion gaps as signatures of strong-coupling insulators in magic-angle twisted bilayer graphene,” *Nature Communications* **14**, 6679 (2023).
 - [47] H. S. Arora, R. Polski, Y. Zhang, A. Thomson, Y. Choi, H. Kim, Z. Lin, I. Z. Wilson, X. Xu, J.-H. Chu, K. Watanabe, T. Taniguchi, J. Alicea, and S. Nadj-Perge, “Superconductivity in metallic twisted bilayer graphene stabilized by wse₂,” *Nature* **583**, 379 (2020).
 - [48] T. J. Boerner, S. Deems, T. R. Furlani, S. L. Knuth, and J. Towns, “Access: Advancing innovation: Nsf’s advanced cyberinfrastructure coordination ecosystem: Services & support,” in *Practice and Experience in Advanced Research Computing*, PEARC ’23 (Association for Computing Machinery, New York, NY, USA, 2023) p. 173–176.
 - [49] C. Wu and S.-C. Zhang, “Sufficient condition for absence of the sign problem in the fermionic quantum monte carlo algorithm,” *Phys. Rev. B* **71**, 155115 (2005).
 - [50] D. J. Scalapino, S. R. White, and S. Zhang, “Insulator, metal, or superconductor: The criteria,” *Phys. Rev. B* **47**, 7995 (1993).

Supplemental Material for “Spin-Polaron Mediated Superconductivity in Doped Chern Antiferromagnets”

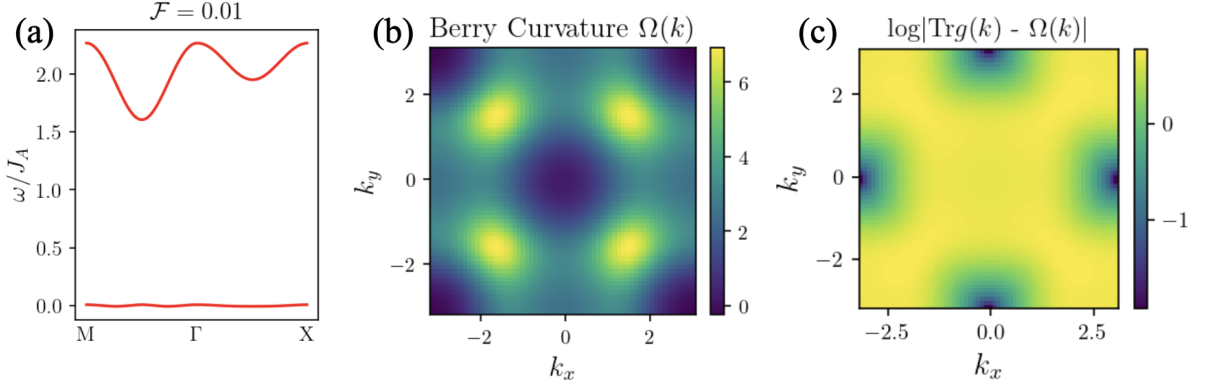
X. Wang, J.F. Mendez-Valderrama, J.S. Hofmann, D. Chowdhury

BAND DISPERSION AND QUANTUM GEOMETRY

As introduced in the main text, the matrices in Eq. 1 that determine the dispersion for the free-particle bands are given by,

$$\begin{aligned} B_{\mathbf{k},\tau=+}^x + iB_{\mathbf{k},\tau=+}^y &= -2t \left[e^{-i\frac{\pi}{4}-ik_y} \cos(k_y) + e^{i\frac{\pi}{4}-ik_y} \cos(k_x) \right] \\ B_{\mathbf{k},\tau=+}^z &= -2t_2 \left[\cos(k_x + k_y) - \cos(k_x - k_y) \right] \\ B_{\mathbf{k},\tau=+}^0 &= -2t_5 \left[\cos(2k_x + 2k_y) + \cos(2k_x - 2k_y) \right] \end{aligned} \quad (S1)$$

where t , t_2 , t_5 are the hopping parameters. For the simulations with $\mathcal{F} = 0.01$, the hopping parameters are given by $t_2 = t/\sqrt{2}$ and $t_5 = (1 - \sqrt{2})t/4$ [13]; whereas for the simulations with $\mathcal{F} = 0.2$, the hopping parameters are given by $t_2 = t/\sqrt{2}$ and $t_5 = 0$, respectively. The non-interacting band structure, associated Berry curvature distribution and deviation from ideal band geometry in the Brillouin zone are shown in Fig. S1.



Supplemental Figure S1. (a) Non-interacting band structure along a high-symmetry cut in the Brillouin zone for $\mathcal{F} = 0.01$. (b) Berry curvature distribution $\Omega(\mathbf{k})$, which is independent of \mathcal{F} since t_5 couples to the identity matrix in sublattice space. (c) Deviation from ideal band geometry in a log-scale. Here $g(\mathbf{k})$ denotes the quantum geometric tensor.

SIGN-PROBLEM-FREE SIMULATION

In this section, we discuss the origin of the sign-problem-free nature of the model defined in Eqn. 1 and 2, respectively. For the auxiliary field quantum Monte-carlo simulations, the presence of an anti-unitary symmetry, $\mathcal{T}' = i\tau_x\sigma_y\mathcal{K}$, is key [49]. Let us re-write the interaction Hamiltonian, $H_{\text{interaction}}$, in Eqn. 2 as,

$$H_{\text{interaction}} = \sum_{\mathbf{r}} \left[J_1 (\mathbf{S}_{\mathbf{r}}^+ + \mathbf{S}_{\mathbf{r}}^-)^2 - J_2 (\mathbf{S}_{\mathbf{r}}^+ - \mathbf{S}_{\mathbf{r}}^-)^2 \right], \quad (S2)$$

where $J_1 = J_A/4 + J_H/2$ and $J_2 = J_A/4 - J_H/2$, respectively. Introducing a Hubbard-Stratonovich decomposition using auxiliary fields, $\phi_{1,\mathbf{r}}$, $\phi_{2,\mathbf{r}}$, in the spin channel, at leading order in $\Delta\tau$, the imaginary-time evolution operator is given by,

$$-\Delta\tau H_{\text{interaction}} = \sum_{\mathbf{r}} \left[\sqrt{-\Delta\tau J_1} \phi_{1,\mathbf{r}} \cdot (\mathbf{S}_{\mathbf{r}}^+ + \mathbf{S}_{\mathbf{r}}^-) - i\sqrt{-\Delta\tau J_2} \phi_{2,\mathbf{r}} \cdot (\mathbf{S}_{\mathbf{r}}^+ - \mathbf{S}_{\mathbf{r}}^-) \right]. \quad (S3)$$

The spin operators in each valley transform under \mathcal{T}' as $\mathcal{T}' S_{\mathbf{r}}^{\pm} \mathcal{T}'^{-1} = -S_{\mathbf{r}}^{\mp}$. It is straightforward to show that if $J_1 > 0$ and $J_2 > 0$, $(-\Delta\tau H_{\text{interaction}})$ is invariant under \mathcal{T}' , which ensures the eigenstates of $H_{\text{interaction}}$ can be grouped into Kramer doublets, guaranteeing the positive-definiteness of the partition function [49]. Similar argument also hold for H_{kin} , and thus the model is sign-problem-free.

SUPPLEMENTARY DATA FOR DETERMINATION OF T_c^{SC}

To characterize the onset of superconductivity, we compute the correlation length,

$$\xi_O \equiv \frac{1}{2 \sin(\pi/L)} \sqrt{\frac{S_O(\mathbf{q}=0)}{S_O(\mathbf{q}=(2\pi/L, 0))}} - 1, \quad (\text{S4a})$$

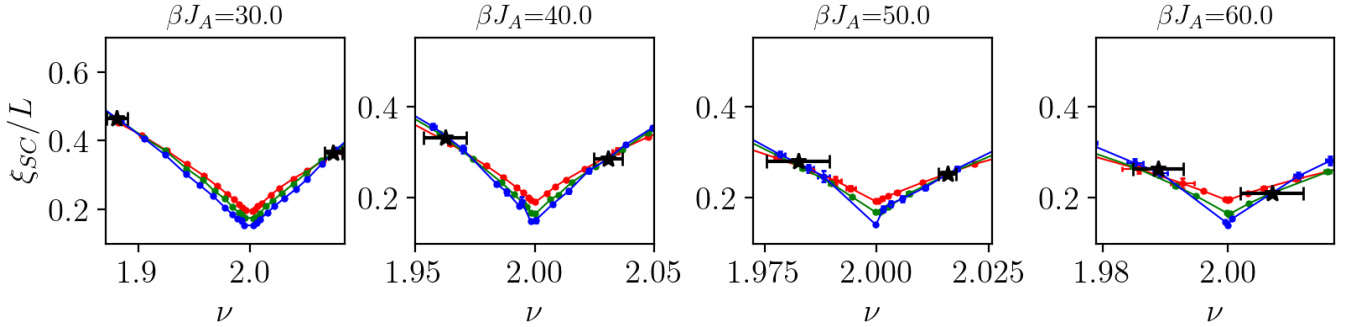
$$S_O(\mathbf{q}) = \frac{1}{L^2} \sum_{\mathbf{r}, \mathbf{r}'} e^{-i(\mathbf{r}-\mathbf{r}') \cdot \mathbf{q}} \langle O^\dagger(\mathbf{r}') O(\mathbf{r}) \rangle, \quad (\text{S4b})$$

where O is the superconducting order parameter defined in Eq. 3a. We also compute the temperature-dependent superfluid stiffness, $\rho_s(T)$, as the transverse electromagnetic response at vanishing Matsubara frequency [50],

$$\rho_s = \frac{1}{4} \langle [-K_{xx} - \Lambda_{xx}(\omega_n, q_y = 0, q_x \rightarrow 0)] \rangle, \quad (\text{S5})$$

where $\Lambda_{xx}(\omega_n, \mathbf{q})$ is paramagnetic current-current correlation, and $K_{xx} \equiv \langle \partial^2 H[\mathbf{A}] / \partial A_x^2 |_{\mathbf{A} \rightarrow 0} \rangle$ is the diamagnetic contribution, with \mathbf{A} the probe vector potential. The superconducting transition temperature, T_c^{SC} , is then determined as $T_c^{\text{SC}} = \pi \rho_s(T \rightarrow T_c^-) / 2$ [36, 37].

We extract the superconducting critical filling ν_c at a fixed inverse temperature β for $|J_H|/J_A = 0.5$ through scaling analysis of ξ_{SC}/L for $h_{\text{SOC}} = 0$ (Fig. S2) and for $h_{\text{SOC}} = 0.01$ (Fig. S3). The superconducting critical filling ν_c at fixed inverse temperature β for $h_{\text{SOC}} = 0.05$ are extracted based on BKT criterion, as shown in Fig. S4.



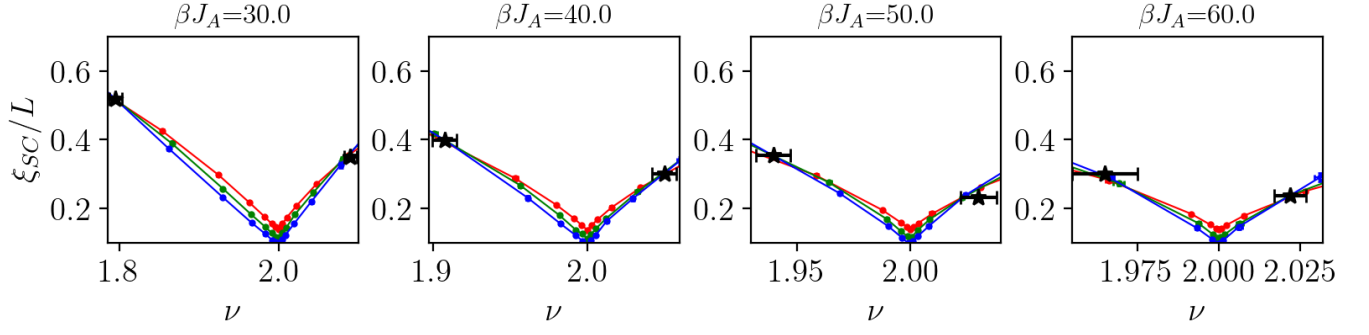
Supplemental Figure S2. Superconducting correlation length ξ_{SC} as a function of ν for $\mathcal{F} = 0.01$, $|J_H|/J_A = 0.5$ and $h_{\text{SOC}} = 0$. Black star with errorbar denotes the critical filling ν_c at the respective temperature. Color schemes are the same as that in Fig. 2a.

We extract the superconducting T_c^{SC} for $|J_H|/J_A = 0.26$ at a fixed ν through BKT criterion for $h_{\text{SOC}} = 0$, as shown in Fig. S5. The filling fractions are fixed through linear interpolation. The superconducting critical filling ν_c at a fixed inverse temperature β are extracted through scaling analysis of ξ_{SC}/L for $h_{\text{SOC}} = 0.01$, as shown in Fig. S6.

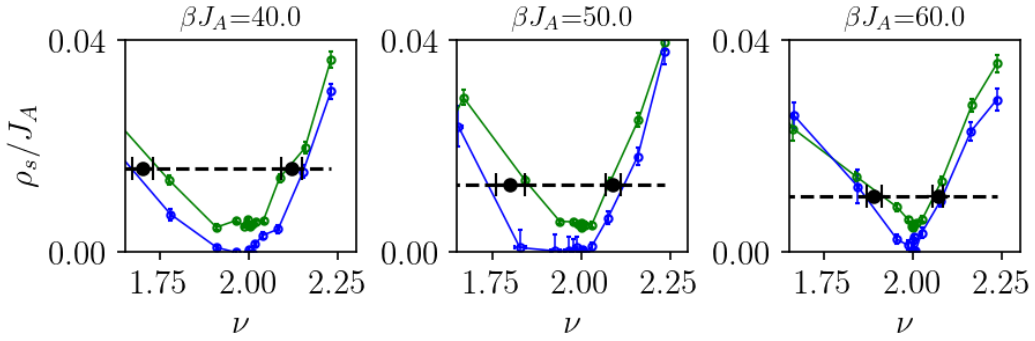
LOW TEMPERATURE BEHAVIOR OF SUPERFLUID STIFFNESS

In this section, we investigate and contrast the low-temperature behavior of the superfluid stiffness in the lightly-doped “skyrmion-mediated” superconductor and the relatively heavily-doped superconductor (where the skyrmions evolve into electrons). We focus on $|J_H|/J_A = 0.5$ and $\mathcal{F} = 0.01$ with $h_{\text{SOC}} = 0$, where we have previously established the existence of skyrmions. We pick $\nu = 2.04$ to probe the skyrmion-mediated superconductor and $\nu = 2.16$ for analyzing the superconductor originating from condensing electronic Cooper pairs.

In Fig. S7(a) and Fig. S7(b), we show the superfluid stiffness $\rho_s(T)$ at $\nu = 2.04$ on a semi-log scale and log-log scale, respectively; we show $\rho_s(T)$ at $\nu = 2.16$ on a semi-log scale in Fig. S7(c). At $\nu = 2.16$, $\rho_s(T)$ saturates exponentially

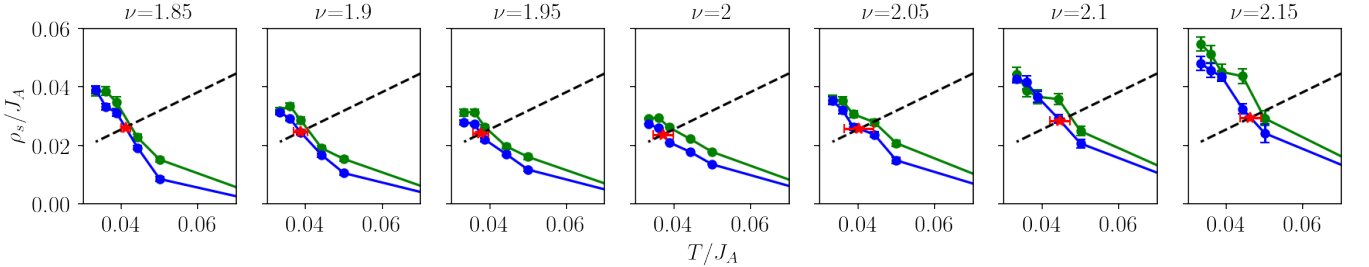


Supplemental Figure S3. Superconducting correlation length ξ_{SC} as a function of ν for $\mathcal{F} = 0.01$, $|J_H|/J_A = 0.5$ and $h_{SOC} = 0.01$. Black star with errorbar denotes the critical filling ν_c at the respective temperature. Color schemes are the same as that in Fig. 2a

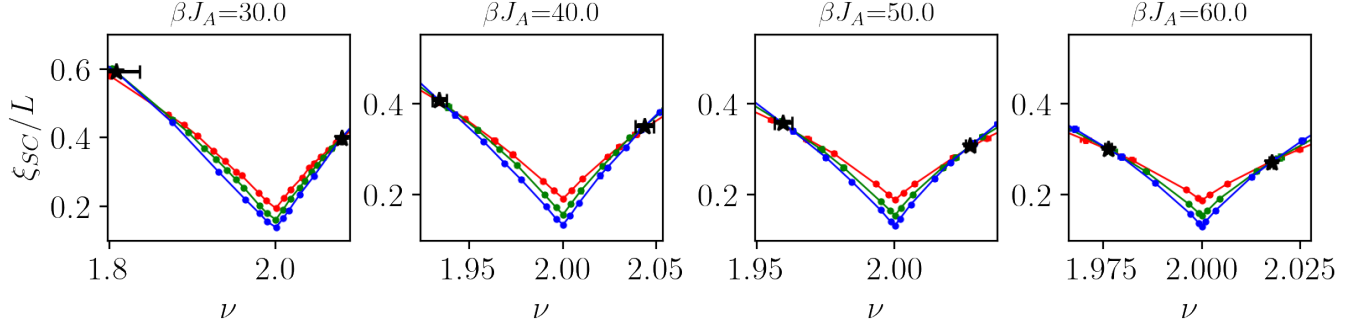


Supplemental Figure S4. Superfluid stiffness ρ_s as a function of varying filling fraction ν , calculated through Eq. S5 for $\mathcal{F} = 0.01$, $|J_H|/J_A = 0.5$ and $h_{SOC} = 0.05$. Color schemes are the same as that in Fig. 2a. Black circle with errorbar denotes the extracted critical filling at respective temperature. Dashed line denotes the BKT line $2T/\pi$.

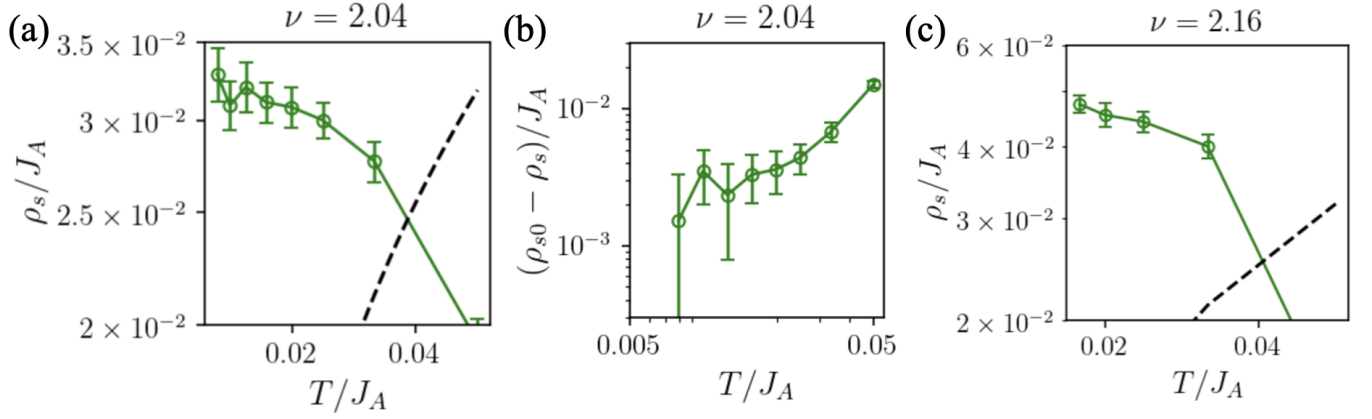
as a function of temperature, which aligns with the expectation for an ordinary fully-gapped superconductor. In contrast, the low-temperature behavior of $\rho_s(T)$ deviates from a clear exponential saturation (Fig. S7a), which is likely due to the existence of gapless fluctuations tied to the CAF order. For the log-log plot of $\rho_s(T) - \rho_s(T = 0)$ in Fig. S7(b), $\rho_s(T = 0)$ is obtained from an extrapolation using a polynomial function. The behavior of $\rho_s(T)$ at $\nu = 2.04$ shows a tendency towards power-law saturation at low temperature. However, to determine the exact scaling, $\rho_s(T = 0)$ should be calculated independently from zero-temperature projective Monte-Carlo simulation, which we leave for future study.



Supplemental Figure S5. Superfluid stiffness ρ_s as a function of varying T at a fixed filling ν , calculated through Eq. S5 for $\mathcal{F} = 0.01$, $|J_H|/J_A = 0.26$ and $h_{SOC} = 0$. Filling fractions are fixed through linear interpolation. Color schemes are the same as that in Fig. 2a. Red star with errorbar denotes the extracted T_c^{SC} at respective filling. Dashed line denotes the BKT line $2T/\pi$.



Supplemental Figure S6. Superconducting correlation length ξ_{SC} as a function of ν for $\mathcal{F} = 0.01$, $|J_{\text{H}}|/J_{\text{A}} = 0.26$ and $h_{\text{SOC}} = 0.01$. Black star with errorbar denotes the critical filling ν_c at the respective temperature. Color schemes are the same as that in Fig. 2a.



Supplemental Figure S7. Saturation of superfluid stiffness at low temperature (a) at $\nu = 2.04$ on a semi-log scale; (b) at $\nu = 2.04$ on a log-log scale; (c) at $\nu = 2.16$ on a semi-log scale. Dashed lines are the BKT lines $2T/\pi$.